American Mineralogist, Volume 72, pages 1241–1250, 1987

Effects of temperature and degree of supersaturation on pyrite morphology

JAMES B. MUROWCHICK, H. L. BARNES
Ore Deposits Research Section, The Pennsylvania State University, University Park, Pennsylvania 16802, U.S.A.

ABSTRACT

The effects of temperature and degree of supersaturation (as controlled by temperature gradient) on the morphology of hydrothermally grown pyrite crystals were investigated over the temperature range from 250 to 500 °C. At a mean temperature of 250 °C and with low supersaturation (temperature gradient of 0.35 °C/cm over 8 cm), needles were produced by the screw-dislocation growth mechanism. As the temperature and/or degree of supersaturation increased (to a mean temperature of 450 °C and a temperature gradient of 4.6 °C/cm and higher over 8 cm), the sequence cube to octahedron to pyritohedron was produced. At extremely high degrees of supersaturation, which occurred during quenching, the growth mechanism shifted from being surface-controlled to diffusion-controlled, causing dendritic growth. Pyrite habit may be used to delineate relatively concentrated zones of nutrient-rich fluid flow.

INTRODUCTION

Eighty-five observed crystal forms ($a\{100\}$, $e\{210\}$, $o\{111\}$, etc.) for pyrite crystals are listed by Dana (1903); Sunagawa (1957) reports seventy-seven from Japan alone, and more than one hundred eighty forms (some of dubious validity) are illustrated in the nearly 700 line drawings of pyrite crystals by Goldschmidt (1920). Apparently, pyrite can occur in a wide variety of habits, possibly more than any other common mineral. However, only three forms make up the majority of pyrite crystals; these are the cube $a\{100\}$, the octahedron $o\{111\}$, and the pentagonal dodecahedron (or pyritohedron) $e\{210\}$ (Fig. 1a). The frequency of occurrence of these three forms is known to vary within many ore deposits and might, therefore, be a practical indicator of conditions in hydrothermal environments. Such use to date has been entirely empirical, with virtually no experimental work to allow general interpretation of pyrite morphologies in relation to ore formation.

Previous work

The discovery that pyrite habit can vary systematically within an ore deposit can be traced back more than thirty years. At least as early as 1952, Amstutz and Ligasacchi (1958) and Amstutz (1963) noticed conspicuous, systematic changes in pyrite morphology from one ore zone or vein to another at Morococha, Peru. However, the mineralization and structure were too complex to permit interpretation at that time. At Cuajone, Peru, the pyrite showed a simple zoning pattern from cubes to pyritohedra with increasing copper values (Amstutz, 1963). At Antimina, Peru, Amstutz noted that pyritohedra occurred in mineralized monzonite and limestone whereas barren granite hosted only cubes, suggesting that pyritohedra and cubes were indicative of ore-forming and non-ore-forming conditions, respectively.

Sunagawa (1957) looked at the distribution of pyrite habits in a large number of Japanese hydrothermal vein and replacement deposits in an attempt to understand the systematics of their variation. He found that the pyritohedral face was sensitive to the mode of occurrence, being $e\{210\}$ in vein-type pyrite, but often consisting of other $\{hk0\}$ forms in replacement deposits. Furthermore, the $\{hk0\}$ indices vary depending on the overall habit: $\{430\}$ associates with $e\{210\}$, $\{540\}$ with the cube, and $\{410\}$ with the octahedron. Sunagawa also found that the habit varied with grain size. In the range of 48 to 8 mesh (0.3 mm to 2.5 mm), the cube was dominant among the smallest grain sizes, the octahedron in the middle sizes, and the pyritohedron in the coarest fraction. From his work at the Yanago mine, he concluded that pyrite grown with "abundant ore solution" shows a greater variety of habits within one grain-size fraction than crystals grown with a "poor supply of ore solution." Furthermore, highly altered host rock shows the greatest variety of habits and the strongest mineralization whereas the least-altered host rock contains only cubes.

The association of different pyrite habits with each of the stages of mineralization at Tintic, Utah, was noticed by Bush et al. (1960). The lower-sulfide-content middle and late barren stages have cubic pyrite, and the sulfide-rich early productive stage has pyritohedra, implying corresponding degrees of supersaturation of the depositing solution.

Possible controls of the habit of pyrite include mechanisms of its crystal growth. Sunagawa's (1957) hypothesis that hydrothermal pyrite crystals grow layer-by-layer on the $a\{100\}$ face according to the mechanism of Kossel (1927) and Stranski (1928) was substantiated by Endo's (1978) study of the surface microtopography of many pyrite crystals. Endo found that, in most cases, pyrite grows by layer spreading (step growth) on the $a\{100\}$ face. The

0003–004X/87/1112–1241$02.00

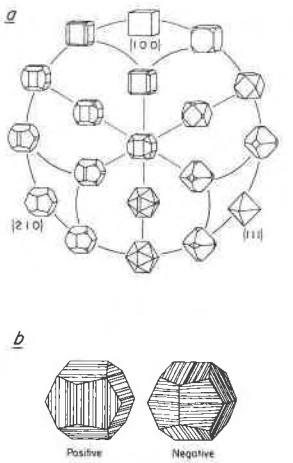

Fig. 1. Common pyrite habits. (a) Habits with forms $a\{100\}$, $o\{111\}$, and $e\{210\}$ (after Sunagawa, 1957). (b) Positively striated (left) and negatively striated (right) pyritohedra (after Endo and Sunagawa, 1973).

habit reflects a high rate of lateral advance of growth layers on {100} and a low rate of initiation of new layers (nucleation on $a\{100\}$). If the rate of nucleation is great enough that young spreading layers can overtake older spreading layers, piling up of the layers will occur. The resulting collection of stepped or kinked layer edges (Hartman and Perdok, 1955) might produce positively striated $e\{210\}$ faces, octahedral faces {111}, or other faces depending on the shape and spreading direction of the $a\{100\}$ layers. In rare cases, layer-by-layer growth can occur on the $e\{210\}$ or $o\{111\}$ faces. Implicitly, increasing the rates of nucleation and layer spreading on the $a\{100\}$ face should promote pyritohedral and octahedral habits. The conditions that would favor such growth would be increased temperature and degree of supersaturation (Gilmer, 1976). This conclusion is in agreement with Sunagawa's (1957) observations.

Other factors may also affect morphology, such as the poisoning of the $o\{111\}$ face by As. A correlation between the As content of the crystal and the increased development of octahedral faces was found by Hayashida and Muta (1952). Sunagawa and Takahashi (1955) also investigated the effect of As on the $o\{111\}$ face by examining samples from six Japanese mines. They concluded that selective adsorption of As on the $o\{111\}$ face does promote the development of that face, but the effect of As can easily be overshadowed by other habit-determining factors. Octahedral crystals without detectable As and high-As crystals lacking the $o\{111\}$ face are well known. Other minor elements (Co, Ni, Se) do not appear to have an effect on the habit of pyrite. Clearly, the effects of trace elements on pyrite morphology need further investigation.

Few experimental studies of pyrite morphology have been conducted. Large (5 mm) crystals of pyrite were grown by Bouchard (1968) in a temperature gradient from 705 to 665 °C over an unspecified distance using Cl_2 gas as the transport agent; however, no investigation of the growth mechanism, habits produced, or the effects of defects was made. Yamada et al. (1979) used Bouchard's method with temperature gradients of 700 to 630 °C and 700 to 400 °C over an unspecified distance. At low gradients, growth was by the layer-by-layer mechanism on $a\{100\}$. Small crystals (up to 0.5 mm) showed $a\{100\}$ faces only; larger crystals also displayed the $o\{111\}$ and $e\{210\}$ faces as well. Growth hillocks on the $o\{111\}$ face were rare. Larger temperature gradients produced wavy rather than straight growth fronts and some twinned crystals. Those results were intriguingly similar to Sunagawa's (1957) and Endo's (1978) observations; however, Yamada et al.'s (1979) crystals were grown by vapor transport and may not accurately reflect growth from hydrothermal solutions.

TABLE 1. Composition of pyrite from the Ward mine, Glendon, North Carolina

Grain size (mm)	>20	20–15	15–10	<10
Fe (wt%)	46.21	44.43	46.46	46.35
S (wt%)	51.38	51.45	51.20	51.09
Acid insol. (wt%)	0.85	1.13	0.98	1.39
Ni (ppm)	170	100	74	52
Co (ppm)	150	72	91	130
Zn (ppm)	24	26	26	24
Cu (ppm)	18	24	12	16
Mn (ppm)	10	10	20	17
Cd (ppm)	<1	<1	<1	<1
H_2O (wt%)	0.11	0.00	0.00	0.00
S/Fe (at. ratio)	1.94	2.02	1.92	1.92
Total (wt%)	98.58	97.01	98.64	98.83

Note: Fe by EDTA titration. S by gravimetric analysis as $BaSO_4$. Acid insolubles and water by gravimetry. Other metals by atomic absorption spectroscopy. Analyses by B. Takano.

Present work

To investigate growth processes and resulting morphologies, our experiments were designed to determine the effects of temperature and degree of supersaturation on the habit of hydrothermally grown pyrite. There is the possibility that the habit of pyrite crystals in a mineralized area could indicate the conditions of mineralization and trends toward areas of most intense mineralization.

Materials and methods

Pyrite crystals were grown using a hydrothermal-transport method utilizing a $5m$ NH_4Cl solution as the transport medium. Crushed natural pyrite from the Ward mine, Glendon, North Carolina, U.S.A. (Table 1), was used as the nutrient in the experiments.

The crystal-growth equipment used in the experiments consisted of three parts: vertically oriented glass capsules containing the crystal-growing environment, an autoclave vessel providing a confining pressure, and a dual-element furnace producing the desired temperature gradients. The autoclave and furnace were designed by Barnes (1971), and only minor modifications have been made since then by Murowchick (1984).

Sealed glass tubes, 7-mm outer diameter by 9 to 10 cm long, were used to enclose the chemical system. The tubes did not react with the contents (NH_4Cl, FeS_2, and H_2O) and permitted

TABLE 2. Pyrite crystal-growth experiments

Run	T_m (°C)	ΔT (°C/cm)	t (d)	Crystal morphology		
				Primary	Pendant	Quench
3	400	0.96	5		0.5-mm $a_s(o)$	
4	450	0.2	14		1–3-mm $a_s(o)$	
10	448	0.4	7	180-μm flat *ao*		50-μm da_s
14	250	0.35	30	60-μm needles		
15	250	6.2	17	34-μm *a*(*o*)		7-μm *aom*
21	450	4.6	5			150-μm o_{sk}, dend
23	450	4.6	5	50-μm $a_s o$	1.2-mm $a_r o$	200-μm $o_{sk}(e,d)$, dend
24	450	2.0	5		150-μm *oa*	150-μm dend, o_{sk}
25	450	2.0	5		200-μm *o*	100-μm dend on *a*
26	450	2.0	5			100-μm dend, o_{sk}
28	350	1.9	10	80-μm $a_s o$		
29	350	1.9	10	42-μm $a_s(o)$		
30	350	1.9	10	75-μm $a_s(o)$		
32	350	2.0	10			280-μm oa_s
34	350	4.0	10	18-μm $a_{(s)}(o)$		
35	350	4.0	10	650-μm *ao*		30-μm a_s
48	400	4.0	10			30-μm o_{sk}, dend
52	385	2.8	0.25	300-μm a_s/o	300-μm $a_s o$	250-μm dend, o_{sk}
53	385	2.8	0.25			250-μm dend, o_{sk}
54	385	2.8	0.25	180-μm a_s/o	300-μm $a_s o$	250-μm dend, o_{sk}
59	416	4.7	9			o_{sk}, dend
60	416	4.7	9			o_{sk}, dend
61	416	4.7	9		2-mm $a_s o$	o_{sk}, dend

Note: T_m = mean run temperature. ΔT = temperature gradient. All runs had a transport distance of about 8 cm for primary crystals and 9 cm for pendant crystals. Time t = duration of run at high temperature. Primary crystals formed at the meniscus at the run temperature. Pendant crystals grew at the top of the capsule nourished by solution lifted during boiling. Quench crystals grew below the high-temperature meniscus during cooling at the end of an experiment. a = {100}, a_s = striated {100}, a_r = rough {100}, o = {111}, o_{sk} = skeletal {111}, m = {311}, d = {110}, e = {210}, a/o = equally developed {100} and {111} forms, ( ) = minor development of form or feature, dend = dendritic.

inspection of the charge without breaking the seal. Vycor glass (96% SiO_2) was used because of its low thermal-expansion coefficient and high softening temperature. Partially constricted tubes closed at one end were loaded with a small amount (ca. 0.1 g) of crushed pyrite (0.1–1 mm) and enough 5*m* NH_4Cl (ca. 3 mL) to cause the meniscus to be about 1 cm from the top of the capsule at the run temperature. (A space for vapor was left at the top of the capsule to prevent failure of the capsule as a result of complete filling and rapid pressure rise resulting from possible overshooting the run temperature during the beginning of an experiment.) The tube was evacuated to the vapor pressure of the NH_4Cl solution and (while under vacuum) sealed at the constriction with a gas torch, the tube being kept cool by wrapping with a wet paper towel.

The stainless-steel autoclave simply provided support pressure for the glass capsules. The autoclave volume was 50 mL, and distilled water was used to provide the support pressure. Because the pressure in the autoclave followed the distilled-water liquid-vapor curve during heating, the pressure in the autoclave was always higher than that within the capsule, which followed the 5*m* NH_4Cl vapor curve.

The thermal gradients were produced by a dual-element furnace, the design of which was such that steep, linear temperature gradients (0.1 to 10 °C/cm at mean temperatures of up to 550 °C) could be maintained when required. Thermocouples inserted at the top and bottom of the autoclave permitted calculation of the temperaure gradient and the temperature at the point of crystal growth. A third thermocouple against the outer surface of the autoclave approximately at its middle was connected to a proportional temperature controller that held the run temperature constant within ±1 °C.

The thermal path of a typical experiment involved rapid heating from room temperature to the run temperature (taking about 2 h) while maintaining a slightly higher temperature at the top of the vessel than at the bottom to prevent transport. After stabilizing the vessel at the run temperature, the thermal gradient was inverted and adjusted to begin convective transport. The duration of the experiments ranged from 6 h to one month at the run temperature. Cooling the vessel at the end of an experiment was hastened by compressed air, bringing the run from 450 to below 100 °C in about 30 min. The crystal products were examined by incident-light microscopy through the walls of the capsules, and differential-interference-contrast and scanning-electron microscopy after opening the capsules. The crystal faces were identified by inspection and comparison with drawings and models with indexed faces.

EXPERIMENTAL RESULTS

The results of the successful runs (Table 2) show that the morphology of pyrite crystals is affected by the temperatures and degree of supersaturation during growth (Figs. 2 and 3). The degree of supersaturation was controlled by the temperature gradient and the distance from the nutrient. Because the distance from the hot nutrient to the cooler meniscus was about the same (8 cm) in all runs, the degree of supersaturation at the point of precipitation was determined by the temperature gradient.

With very low temperature gradients (0.2–0.35 °C/cm), needles were produced at 250 °C (run 14, Fig. 2c), whereas at 450 °C, large striated cubes with small octahedral

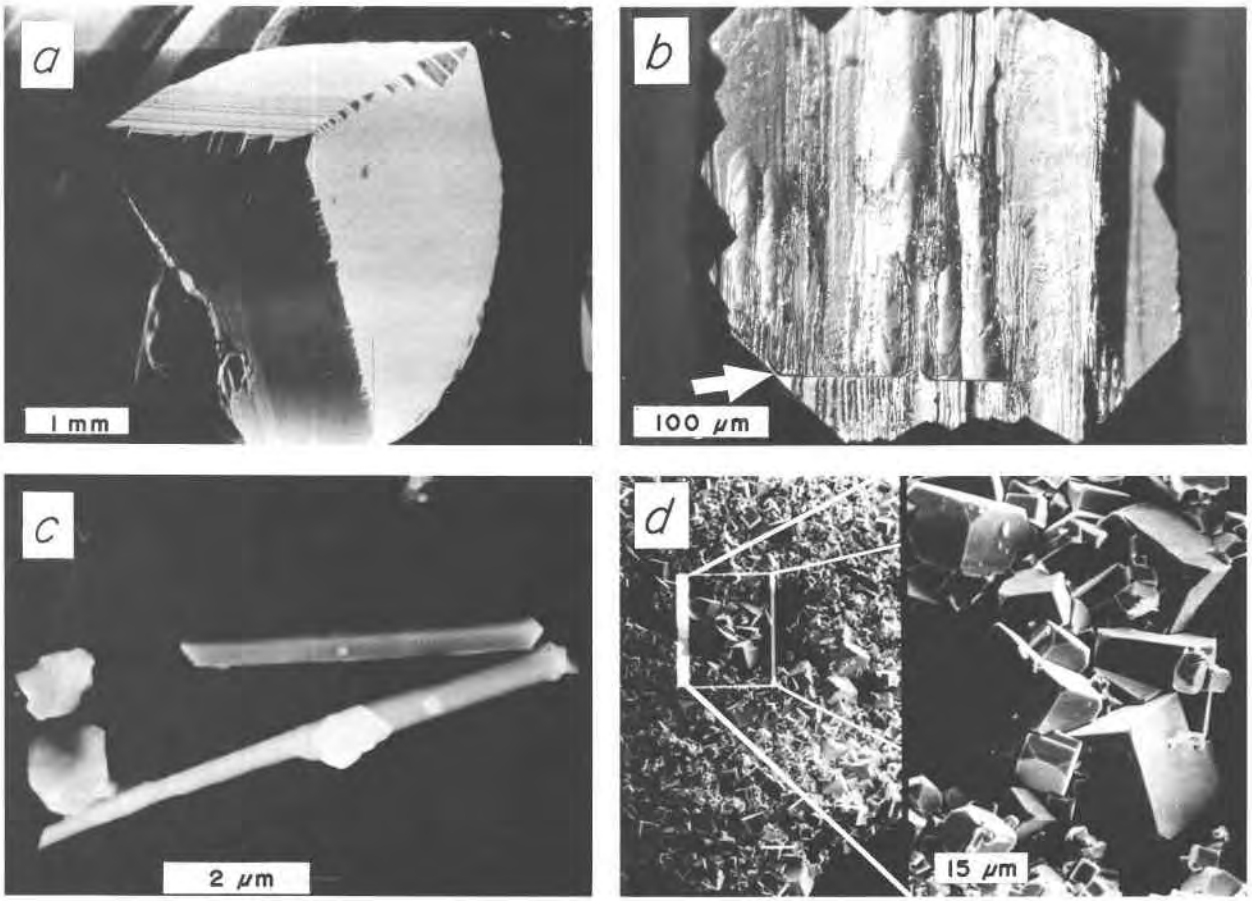

Fig. 2. Pyrite crystals grown under steady-state conditions. (a) Lightly striated cube grown at a mean temperature of T_m = 450 °C and a temperature gradient of 0.2 °C/cm over 8 cm. (b) Heavily striated cube grown at T_m = 450 °C and 4.6 °C/cm over 8 cm. Note the development of growth hillocks, domains [horizontal cube faces (arrow) near the bottom of the crystal], and $o\{111\}$ faces. (c) Needles grown at T_m = 250 °C and 0.35 °C/cm over 8 cm. (d) Perfectly smooth cubes with small $o\{111\}$ faces grown at T_m = 250 °C and 6.2 °C/cm over 8 cm.

faces were formed (run 4, Fig. 2a). Larger temperature gradients (5–6 °C/cm) at 250 °C resulted in cubes with perfectly smooth $a\{100\}$ faces and small $o\{111\}$ faces (run 15, Fig. 2d). The combination of high temperatures with large gradients produced heavily striated cubes with or without the development of octahedral faces (runs 23 and 61, Fig. 2b). Defects and domain structures are more common in the crystals grown at high temperature (450 °C).

Crystals that grew during the period of rapid cooling at the end of each run showed habits that varied according to their position within the capsule (Fig. 3). The general sequence of quench-crystal morphology from the cooler top to the hotter bottom was as follows: Blocky crystals (often cubes) occurred from 0.5 to 1.0 cm below the meniscus downward to about 2 cm below the meniscus. Beginning slightly below the blocky-crystal zone, octahedra and skeletal octahedra extended about 1 cm or so down the capsule. Dendritic pyrite crystals began below the top of the zone of octahedra and extended downward coating the earlier crystals. The lowest zone was composed of very fine grained iron sulfides. Though not positively identified in every run, these included pyrrhotite, pyrite, greigite, or an amorphous phase as permitted by the chemistry of the system.

Runs in which a small pyrite seed was suspended on a thin Pt wire met with little success. Different methods of attachment of the crystal to the wire were tried, but the crystal either dissolved or fell off the wire. The Pt wire, however, sometimes favored nucleation.

Most runs were unsuccessful because of capsule failure, lack of crystal nucleation, or the occurrence of boiling within the capsule (75% of the first 20 runs were lost due to capsule failure caused by dissolution or recrystallization of the capsule). Subsequent modifications reduced the capsule failure rate, but the overall failure rate remained at 75% for the remaining 50 runs because of lack of crystal nucleation. Boiling within the capsule during an experiment resulted in the growth of a few very large crystals at the top of the capsule with or without the growth

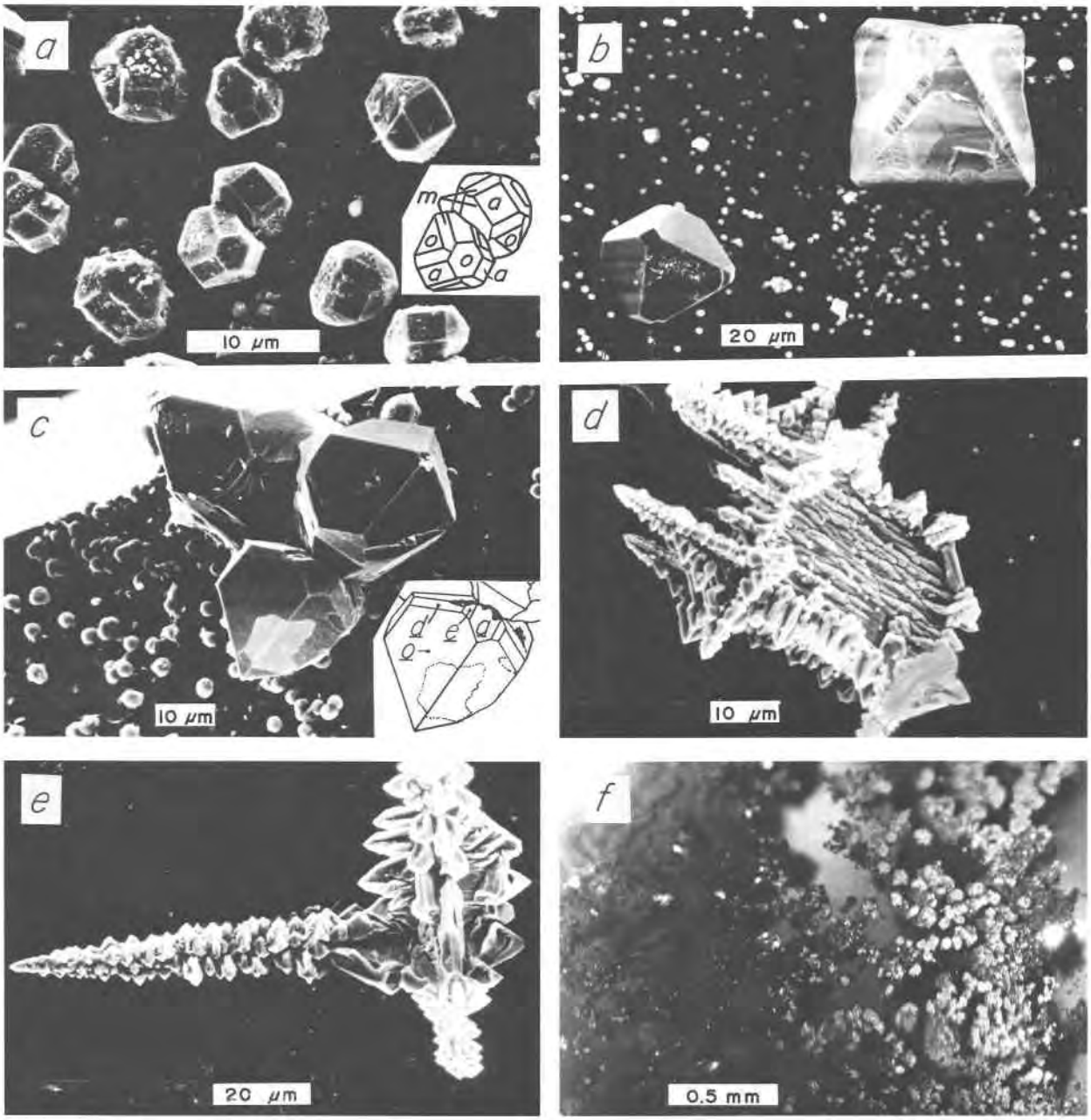

Fig. 3. Pyrite crystals grown during quenching. The sequence (a) through (f) illustrates the change in morphology as the degree of supersaturation increased during cooling. In (a), the solution was cooled from 250 °C; in (b) through (f), the solution was cooled from 400 or 450 °C to room temperature. (a) Blocky crystal displaying $a\{100\}$, $o\{111\}$, and $m\{311\}$ forms. (b) Octahedra. The larger crystal has slightly hollowed $\{111\}$ faces, indicating that the transition from surface-controlled to diffusion-controlled growth had begun. (c) Skeletal octahedron with small $a\{100\}$, $e\{210\}$, and $d\{110\}$ forms (see inset). (d) Dendritic growth on an earlier-formed cube. Note that the dominant direction of growth is still perpendicular to the cube faces. (e) Dendrite with three orthogonal branches. The individual crystallites are hollow-faced octahedra. (f) Very fine grained precipitate (pyrite, pyrrhotite, or amorphous FeS). Photographs (a) through (e) are SEM photomicrographs; (f) is an incident-light photomicrograph taken through the wall of the capsule.

of flat crystals along the sides above the position of the high-temperature meniscus.

Many of the later runs, which were cooled much more quickly than earlier runs (cooled in 30 min as opposed to several hours), produced two liquids after cooling, a yellow one above a colorless one. Mixing of the two liquids immediately produced a dense, black precipitate which settled to the bottom of the capsule. The precipitate was

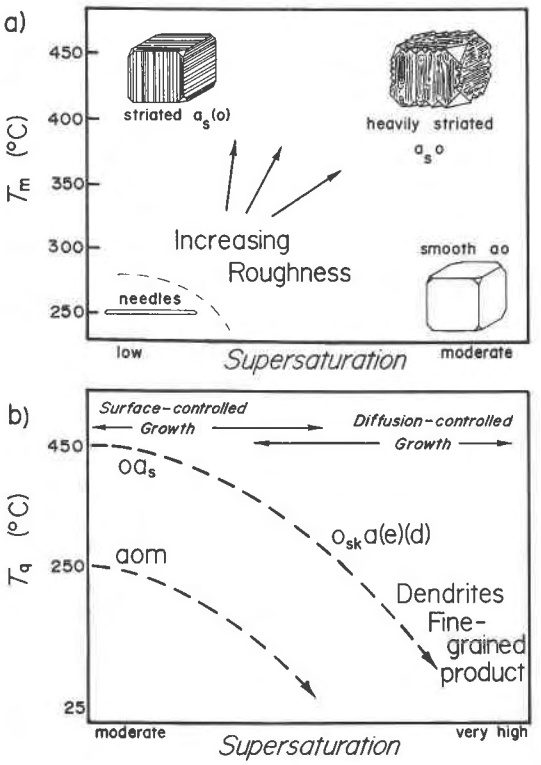

Fig. 4. Morphologies of hydrothermally grown pyrite. (a) Habits produced during steady-state conditions. T_m is the mean run temperature. The degree of supersaturation is known only approximately for this system. (b) Typical temperature vs. supersaturation paths (heavy dashed lines) and habits produced during quenching. T_q is the temperature at the beginning of the quench. Crystal forms are given in decreasing order of development using the letters $a = \{100\}$, $o = \{111\}$, $e = \{210\}$, $m = \{311\}$, and $d = \{110\}$. Subscripts s and sk indicate the associated forms are striated or skeletal, respectively, and parentheses indicate minor development of the form or feature.

not identified because of its small quantity, but was most likely an amorphous iron sulfide phase. To determine whether the phenomenon was the result of liquid immiscibility or simply represented a condensed vapor phase on top of the liquid phase, a double-tube capsule was constructed. The inner, open capsule's volume was such that at the temperature of the experiment, the inner capsule was filled nearly to the brim with liquid, thus minimizing the amount of vapor phase that could collect in the inner capsule during quenching. Upon cooling, the vapor phase condensed to a yellow liquid that collected in the outer capsule. The original liquid phase (colorless) remained in the inner capsule together with a small amount of condensate (yellow). The quench test with this configuration showed that the yellow liquid was a condensate and not an immiscible second liquid at high temperature. The ratio of the volumes of the yellow and colorless liquids was not constant, but depended on the initial liquid-to-vapor ratio in the capsule.

Discussion

The crystals grown during the transport experiments clearly show a relationship between the habit and/or surface structure of the crystal and the growth conditions, specifically the temperature and degree of supersaturation (Fig. 4). There are two generations of pyrite: (1) primary crystals that grew during the main steady-state part of an experiment and (2) quench crystals that grew during the cooling stage at the end of an experiment. The two generations are distinguished by their location in the capsule and their morphologies: primary crystals formed mostly near the high-temperature meniscus, and had well-formed, complete faces. Crystals formed during the cooling cycle at the end of an experiment formed only below the position of the meniscus at a particular time during the cooling cycle, usually displayed incomplete faces and dendritic forms, and often grew on older primary crystals. The observed changes in habits of these two generations are consistent with the crystal-growth mechanisms proposed by Sunagawa (1957, 1981) and Endo (1978).

There are several general mechanisms of crystal growth from aqueous solutions that operate within different temperature ranges and degrees of supersaturation. Simplified, these are the screw-dislocation, layer-by-layer, and continuous growth mechanisms, but only the first two are important here. These mechanisms are described in detail by Nielson (1964), Ohara and Reid (1973), and others and will be only briefly reviewed for our purposes.

At very low degrees of supersaturation, screw-dislocation–controlled growth (Burton et al., 1951) can be the dominant growth mechanism. A screw dislocation that emerges at the surface of the crystal will produce a step on the growing face. Incorporation of atoms into the crystal structure is favored along the step (two bonding neighbors) over attachment to the flat face (only one bonding neighbor) so that the edge advances as growth occurs. Because the end of the step is tethered at the dislocation, the growth edge advances by spiraling around the dislocation. An excellent computer simulation of this process is given in Gilmer (1976). The continuous migration of the growth front up the spiral ramp results in crystals that grow rapidly in the direction of the dislocation, often resulting in acicular habits.

At higher degrees of supersaturation, nucleation on the growing surface and lateral spreading from these nuclei become the dominant growth mechanism. This two-dimensional, layer-by-layer growth was originally described by Kossel (1927) and Stranski (1928). At low degrees of supersaturation, the rate of nucleation on the surface is low. A layer can spread laterally to the edge of the crystal in a relatively short time, but formation of a new layer is limited by the rate of formation of new nuclei. (This "dead time" during growth does not occur when the screw-dislocation mechanism is dominant.) As the temperature or degree of supersaturation increases, however, the rate of nucleation of new layers also increases. Correspondingly, the layer-by-layer mechanism eventu-

ally becomes dominant and contributes to the crystal growth faster than the screw-dislocation mechanism (Gilmer, 1976).

At very high degrees of supersaturation, the surface of the crystal can become quite rough on an atomic scale, and the rate of nucleation then becomes extreme (Kirkpatrick, 1975). The continuous growth mechanism can dominate under these conditions, but is usually observed when the surface structure of the crystal is similar to that of the growth medium and the latent heat of crystallization is low. Such conditions are most commonly found in melts rather than aqueous systems and were not important in these experiments.

The rate of crystal growth can be limited by either the rate at which components are incorporated into the growing surface (surface-controlled growth, Fig. 5a) or the rate at which those nutrient components diffuse to the surface (diffusion-controlled growth, Fig. 5b). Surface-controlled growth commonly occurs in aqueous systems because of the higher diffusion rates than nutrient-incorporation rates in aqueous solutions. Corners and edges do not grow faster than flat faces because the nutrient is evenly distributed around the crystal and the corners and edges do not protrude into regions of higher supersaturation. Equant, euhedral crystals are typically the result.

During the diffusion-controlled growth, the concentration of nutrient increases away from the surface of the crystal. Any protrusion of the crystal surface may cross concentration contours to encounter higher supersaturation than at other portions of the crystal surface. Growth at the end of the protrusion will be favored over growth on the flat surface and a dendrite will be produced (see McLachlan and Carlson, 1952). The dendrite will create its own concentration gradient around itself, inhibiting the growth of other dendrites within some small distance from the first. A common result is a set of evenly spaced dendrites, each with evenly spaced branches. McLachlan and Carlson (1952) give a quantitative model of this type of growth.

The results of the crystal-growth experiments can be understood in terms of the two growth-controlling processes just described. During the steady-state part of an experiment, the degree of supersaturation remained low enough (and the growth rates were low enough) that the rates were surface-controlled. Crystals showing the cubic and octahedral faces were common (Fig. 2). At a mean temperature of 250 °C and a gradient of 0.35 °C/cm over 8 cm, the degree of supersaturation was low enough for the screw-dislocation mechanism to dominate, producing the acicular crystals shown in Figure 2c. Increasing the degree of supersaturation at the same temperature (250 °C, 6.2 °C/cm over 8 cm) caused the layer-by-layer mechanism to become dominant, producing the smooth cubes in Figure 2d.

Increasing the temperature had a similar effect: at a mean temperature of 450 °C and a gradient of 0.2 °C/cm over 8 cm, lightly striated cubes formed (Fig. 2a), indicating that layer-by-layer growth was the dominant mechanism under those conditions as well. Even at a mean temperature of 450 °C and a gradient of 4.6 °C/cm over 8 cm, surface-controlled layer-by-layer growth was the dominant growth mechanism, as indicated by the crystals in Figure 2b.

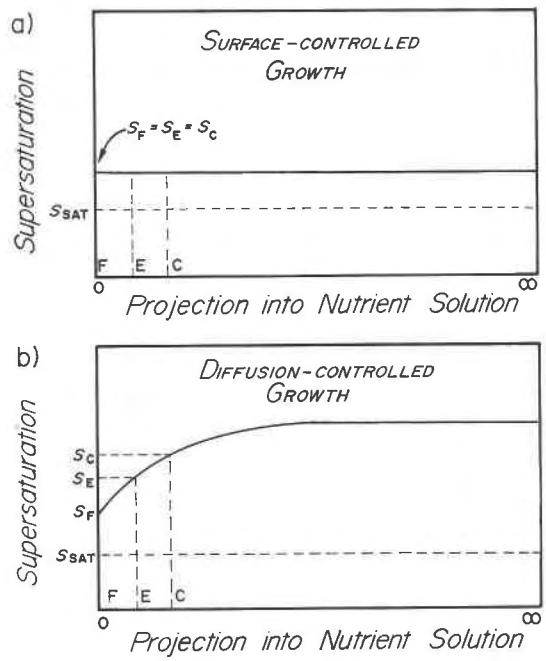

Fig. 5. Schematic concentration profiles during surface- and diffusion-controlled growth. (a) During surface-controlled growth, the degree of supersaturation (S) does not vary appreciably from the surface outward into the bulk of the solution. Therefore, the supersaturation (S) at the growing face (F), edge (E), and corner (C) are the same ($S_F = S_E = S_C$). S_{sat} is saturation. (b) During diffusion-controlled growth, the degree of supersaturation decreases as the crystal is approached. The corners consequently grow under conditions of greater supersaturation than the edges and the faces ($S_C > S_E > S_F$). Competition for nutrients leads to preferential growth of the corners and edges at the expense of growth on faces (see Fig. 3d).

For most natural pyrite crystals grown from hydrothermal solutions, their morphologies indicate that they grow by two-dimensional nucleation and spreading on the $a\{100\}$ face (Sunagawa, 1957; Endo and Sunagawa, 1973; Feklichev and Alisev, 1973). If the rate of nucleation becomes great enough, the spreading layers will tend to pile up on one another, producing larger growth steps. This piling-up process can result in the formation of striae (usually parallel to the edge between $a\{100\}$ and $e\{210\}$), $o\{111\}$, $e\{210\}$, $m\{311\}$, $d\{110\}$, and many other less important forms.

In the synthetic pyrite crystals in Figure 2, the piling-up of layers is manifested as striae and $\{111\}$ faces. Increasing the temperature or degree of supersaturation results in better-developed striae and $o\{111\}$ faces. However, the $e\{210\}$ and other minor faces did not appear among the primary crystals for reasons to be discussed below.

During the cooling period at the end of a run, several

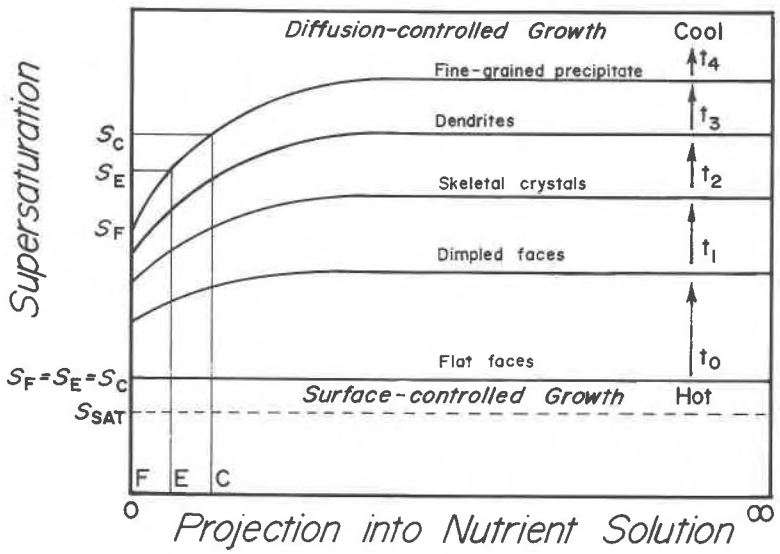

Fig. 6. Schematic profiles of nutrient concentration during quenching. At the inception of cooling at the end of an experiment (t_0), the supersaturation profile was typical of surface-controlled growth ($S_F = S_E = S_C$). As cooling progressed (t_1 to t_4), the profile gradually shifted to that resulting from diffusion-controlled growth ($S_C > S_E > S_F$), explaining the shift from the formation of complex, euhedral crystals at the beginning of the cooling cycle to dendritic growth as cooling continued.

processes occurred simultaneously: the solution contracted, the degree of supersaturation increased rapidly, and the crystal growth rate shifted from dominantly surface-controlled to dominantly diffusion-controlled. At the beginning of the quench process ($t = t_0$, Fig. 6), the solution was about as supersaturated as during the run. As the solution cooled ($t = t_1$ to t_4), the degree of supersaturation increased rapidly. As new crystals nucleated, their growth rate increased according to a power function of the degree of supersaturation (see Ohara and Reid, 1973). The first-formed crystals developed faces, indicating that the growth rate was still surface-controlled. The dimpling of the $o\{111\}$ faces on the large octahedron in Figure 3b indicates that the transition to diffusion-controlled growth was taking place. The transition is gradual from dominantly surface- to diffusion-controlled. As cooling continued, the apices of the octahedra received more nutrient than the faces. Growth on the face (or [110] spreading of $a\{100\}$ layers to form the $o\{111\}$ face) was inhibited by nutrient depletion ccaused by growth of the apices and edges; skeletal octahedra (Fig. 3c) were the result.

The growth process became even more extreme as cooling progressed. The skeletal octahedra were succeeded by dendrites, the crystallites of which were themselves skeletal octahedra (Figs. 3d and 3e). Note that the dendrites grew only in the [100] directions (Fig. 3d). Endo (1975) found the same phenomenon in natural dendritic pyrite from the Ani mine, Akita Prefecture, Japan. Even though the growth process changed from surface reaction to diffusion, the growth mechanism was still layer-by-layer growth on the $a\{100\}$ faces (the slowest-growing faces are preserved). The final product during cooling was a fine-grained sulfide without any distinctive crystal shape (Fig. 3f). The material was not analyzed, but probably was pyrite, pyrrhotite, greigite (at low temperatures), or an amorphous phase. If it was pyrite, then the possibility exists that the continuous growth mechanism became dominant. A more likely explanation is that saturation with respect to another phase (pyrrhotite, greigite, etc.) was exceeded, causing precipitation of that phase.

The question of the scarcity of the $e\{210\}$ form among the synthetic crystals remains. The cause may also apply to the low frequency of other faces ($m\{311\}$ and $d\{110\}$) in the experiments. In Figure 3c, $e\{210\}$ and $d\{110\}$ faces are present in the quench products, but poorly developed. Based on their locations, they occur where the solution must have had a diminished degree of supersaturation compared to that at the apices, but not as low as that at the center of the $o\{111\}$ face. The degree of supersaturation probably exceeded that due to the temperature gradient in the steady-state period of the experiments. The conditions during cooling permitted formation of the $e\{210\}$ face, but the change from surface-controlled to diffusion-controlled growth led to the runaway formation of dendrites and inhibited the development of any flat crystal faces, including $e\{210\}$. The $m\{311\}$ face (Fig. 3a) also formed under conditions of greater supersaturation than was maintained under steady-state conditions. The main difference between the $e\{210\}$ and the $m\{311\}$ faces in Figures 3a and 3c is that the former formed during cooling from a mean temperature of 250 °C whereas the latter formed during cooling from a mean temperature of 450 °C. Higher degrees of supersaturation were reached during cooling from 450 °C than from 250 °C, promoting the formation of the $e\{210\}$ faces.

The implications of the two liquids observed in some

runs and their effect on the results of the experiments is only partly understood. The yellow color of the condensate at room temperature suggests the presence of polysulfides (dominantly S_n^{2-}, HS_n^- or H_2S_n, $n = 2$–6). The disparity in the pH value of the condensate and the colorless liquid (8.4 vs. 4.0, respectively) may be due to the fractionation of NH_3 into the vapor phase, leaving behind an HCl solution that ionizes to become acidic on cooling:

$$NH_4Cl \rightleftharpoons NH_{3(g)} + HCl_{(aq)}. \quad (1)$$

The dissolving nutrient pyrite produced H_2S and polysulfides:

$$xFeS_2 + 2xH^+ \rightleftharpoons xFe^{2+} + (x - 1)H_2S + H_2S_{(x+1)}. \quad (2)$$

The polysulfides may have fractionated into the more alkaline, NH_3-rich vapor phase to a greater degree than did the H_2S, causing the H_2S/H_2S_n ratio to increase in the remaining liquid. The remnant Fe^{2+}-enriched liquid was so depleted of S^0 (in polysulfides) in some of the experiments that pyrrhotite (identified by crystal morphology and optical properties) precipitated instead of pyrite, supporting this possibility. The ratio of the volumes of the condensate to the liquid phase varied depending on the initial degree of filling, the concentration of the NH_4Cl solution, and the temperature of the run. The ratio of condensate to colorless liquid increased with decreasing NH_4Cl concentration, increasing run temperature, or decreasing initial degree of filling. The effect of the varying fluid ratio on the transport and morphology of the growing crystals was not evident. Either removal of S^0 from the solution or lowering of the pH should decrease the degree of supersaturation with respect to pyrite.

Comparisons with natural crystals

Acicular pyrite is rare in nature, but is known to occur at Naica, Chihuahua, Mexico (White, 1973), Haledon, New Jersey, and in geodes from Hall's Gap, Kentucky (Bideaux, 1970). These occurrences, along with the experimentally grown needles in this study, indicate that the acicular habit is produced under conditions of low supersaturation and low to moderate temperatures ($\leq$250 °C).

Part or all of the sequence cube to octahedron to pyritohedron occurs from barren country rocks into a mineralized hydrothermal vein (Sunagawa, 1957). This sequence is consistent with the observation that as the degree of supersaturation increases, the habit changes from cubes to octahedra to pyritohedra. Pyrite crystals growing from a flowing fluid in an open vein are unlikely to have diffusion-controlled growth; true dendritic growth is therefore uncommon in hydrothermal veins (Endo, 1975). Pyrite dendrites have been observed where fluids were stagnant in a submarine hydrothermal chimney at lat 13°N on the East Pacific Rise (U. Graham and H. Ohmoto, pers. comm., 1987).

Temperature gradients as steep as those used in this study are not common in nature (except in sea-floor geothermal systems), but the high degrees of supersaturation needed to grow equidimensional, euhedral forms other than cubes (including {111}, {210}, {110}, and {310}) can be produced by a variety of natural chemical processes. For example, if a hydrothermal solution in equilibrium with pyrrhotite at depth isothermally ascends to mix with oxidizing groundwater, part of the sulfide species in solution (H_2S, HS^-) can be oxidized to form S_2^{2-} or HS_2^- at the pH values of interest in this work:

$$2H_2S_{(aq)} + \tfrac{1}{2}O_{2(aq)} \rightleftharpoons HS_2^- + H_2O + H^+ \quad (3a)$$

$$2HS^- + \tfrac{1}{2}O_{2(aq)} \rightleftharpoons S_2^{2-} + H_2O. \quad (3b)$$

Only a very small portion of the sulfide in solution needs to be oxidized to saturate the solution with respect to pyrite. Further oxidation could produce very high degrees of supersaturation with respect to pyrite; conditions such as these may favor the formation of pyritohedra. There are several other chemical processes that can produce high degrees of supersaturation in hydrothermal systems (pH change, dilution, loss or addition of reactants, etc.), and combinations of these may account for the frequency of pyritohedra and other noncubic forms in many ore deposits.

The distribution of pyrite zoning by habit, and the significance of the various habits as geochemical indicators, is not yet well enough understood to support its use as a general exploration tool except in a few cases (e.g., Arifulov, 1978; Evzikova and Belan'kaya, 1980). In those cases, the relation of pyrite habit to ore mineralization was established by empirical observations in specific deposits and might not apply to other deposits. Before a quantitative and predictive understanding of the controls on pyrite morphology can be acquired, further experiments are needed. Some proposed improvements in these experiments follow. Boiling of the transport solution occurred when the temperature gradient was large enough, allowing large crystals to form at the very top of the capsule. Growth rates were rapid, producing 4-mm crystals in 5 d, but the growth conditions were not well defined because of variable boiling. To prevent boiling, the temperature gradient should be inverted so that the top of the capsule is hotter than the bottom. Such a configuration would also prevent the formation of stacked convection cells within the capsule (see Rising, 1973), promoting a more linear temperature gradient. The nutrient material should then be suspended from the top of the capsule (e.g., with a Pt wire) so that immersion of the nutrient during solution expansion does not occur until the run temperature is reached. If the top of the capsule is kept slightly cooler than the bottom until the gradient is inverted at the beginning of the experiment, transport will not occur during the heating period.

A small degree of supersaturation is required for nucleation to take place. In many of the experiments of this study, primary pyrite did not nucleate, possibly because the required critical supersaturation was not reached. The use of a seed crystal should promote crystal formation because the degree of supersaturation required for growth is much lower than that required for nucleation. Seeds

can be introduced before the capsule is sealed, but the large size of the seeds compared to the primary crystals (especially at low temperatures) might produce an unwanted predisposition toward certain habits. Pt wire appeared to promote nucleation in some of the runs and might be a useful substrate. Another method would be to overheat the capsule by 25–50 °C and then quench it to the run temperature. The formation of quench crystals should provide an adequate supply of small, uniformly sized seeds.

Conclusions

Growth temperature and degree of supersaturation have profound effects on the morphologies of hydrothermally grown pyrite crystals. Low degrees of supersaturation at temperatures below about 250 °C produced acicular crystals presumably by a screw-dislocation growth mechanism. Higher degrees of supersaturation at 250 °C produced perfectly smooth cubes. At 450 °C, low degrees of supersaturation produced lightly striated cubes with small octahedral faces whereas higher degrees of supersaturation resulted in the formation of rough cubes, increased development of the octahedral form, and (in quench crystals) pyritohedral and trapezohedral forms. A surface-controlled growth process led to the formation of complex euhderal crystals; diffusion-controlled growth resulted in skeletal and dendritic habits. A general sequence of forms indicating increasing degree of supersaturation is, then, cube to octahedron to pyritohedron. Forms such as {110} and {311} are less common than these three, but seem to fit into the sequence between the octahedral and pyritohedral forms. Mapping of pyrite habit could delineate zones of high supersaturation of hydrothermal fluids, and hence, zones of potential mineralization. Though this has been used empirically, there clearly is a kinetic basis for such zonation.

Acknowledgments

We thank D. K. Smith, A. C. Lasaga, R. E. Newnham, and A. W. Rose for their many helpful discussions and comments during the course of this work. C. A. Francis, R. I. Gait, and M. F. Hochella, Jr., reviewed this paper; their comments and suggestions are greatly appreciated. Financial support was provided by National Science Foundation Grants EAR-7713073 and EAR-8206777 to H.L.B., a Mining, Mineral, and Mineral Fuel Conservation Fellowship to J.B.M., and the Ore Deposits Research Section of The Pennsylvania State University.

References cited

Amstutz, G.C. (1963) Accessories on pyrite, pyrite zoning, and zoned pyrite. Schweizerische Mineralogische und Petrographische Mitteilungen, 33, 111–122.

Amstutz, G.C., and Ligasacchi, A. (1958) Mineralization zoning based on habit changes of pyrite (abs.). Geological Society of America Bulletin, 69, 1529–1530.

Arifulov, Ch. Kh. (1978) [Genetic types of pyrite and their use for evaluating the gold content in the sulfide mineralization zone] (in Russian). Deposited Documents, VINITI 482-78, 36–43.

Barnes, H.L. (1971) Investigations in hydrothermal systems. In G.C. Ulmer, Ed., Research techniques for high pressure and temperature, chap. 12, p. 317–355. Springer-Verlag, New York.

Bideaux, R.A. (1970) Mineral rings and cylinders. Mineralogical Record, 1, 105–112.

Bouchard, R.J. (1968) The preparation of single crystals of FeS_2, CoS_2, and NiS_2 pyrites by chlorine transport. Journal of Crystal Growth, 2, 42–44.

Burton, W.K., Cabrera, N., and Frank, F.C. (1951) The growth of crystals and the equilibrium structure of their surfaces. Royal Society of London Philosophical Transactions, A243, 299–353.

Bush, J.B., Cook, D.R., Lovering, T.S., and Morris, H.T. (1960) The Chief Oxide–Burgin area discoveries, East Tintic district, Utah; A case history—Pt. 1, U.S.G.S. studies and exploration. Economic Geology, 55, 1116–1147.

Dana, E.S. (1903) The system of mineralogy of James Dwight Dana, 6th edition, p. 84. Wiley, New York.

Endo, Y. (1975) Morphological features and growth process of dendritic pyrite from Ani mine, Akita Prefecture. Prof. T. Takéuchi Memorial Volume, p. 15–18 (not seen; extracted from Mineralogical Abstracts, 1979, abs. no. 79-4092).

——— (1978) Surface microtopographical study of pyrite crystals. Geological Society of Japan Bulletin, 29, 701–745.

Endo, Y., and Sunagawa, I. (1973) Positive and negative striations in pyrite. American Mineralogist, 58, 930–935.

Evzikova, N.Z., and Belen'kaya, N.S. (1980) [Change in the shape of pyrite crystals in ore bodies] (in Russian). Novye Dannye Tipomorfizme Mineralov, 1980, 80–89.

Feklichev, V.G., and Alisev, R.M. (1973) [Crystal morphology of pyrite] (in Russian). Zapiski Vsesoyuznogo Mineralogicheskogo Obshchestva, 102, 194–198.

Gilmer, G.H. (1976) Growth on imperfect crystal faces I. Monte-Carlo growth rates. Journal of Crystal Growth, 35, 15–28.

Goldschmidt, V. (1920) Atlas der Kristallformen, Bd. 6, Markasit-Pyrit, p. 179–208, plates 101–144. Carl Winters Universitätbuchhandlung, Heidelburg.

Hartman, P., and Perdok, W.G. (1955) On the relation between structure and morphology of crystals, I, II, and III. Acta Crystallographica, 8, 49–52, 521–529.

Hayashida, S., and Muta, K. (1952) [Relation of trace-element content and crystal form in pyrite] (in Japanese). Journal of the Mining Institute of Kyushu, 20, 233–238.

Kirkpatrick, R.J. (1975) Crystal growth from the melt: A review. American Mineralogist, 60, 798–814.

Kossel, W. (1927) Zur theorie des Kristallwachstums. Nachrichten von der Gesellschaft der Wissenschaften zu Göttingen, 2, 135–145.

McLachlan, D., Jr., and Carlson, A. (1952) Some factors in the growth of crystals: Part II. Dendritic growth. University of Utah Engineering Experiment Station Bulletin, 57, 24–28.

Murowchick, J.B. (1984) The formation and growth of pyrite, marcasite, and cubic FeS. Ph.D. dissertation, The Pennsylvania State University, University Park, Pennsylvania, 168 p.

Nielson, A.E. (1964) Kinetics of precipitation. Pergamon Press, Oxford, England.

Ohara, M., and Reid, R.C. (1973) Modeling crystal growth rates from solution. Prentice-Hall, Englewood Cliffs, New Jersey, 272 p.

Rising, B.A. (1973) Phase relations among pyrite, marcasite, and pyrrhotite below 300°C. Ph.D. dissertation, The Pennsylvania State University, University Park, Pennsylvania, 192 p.

Stranski, I.N. (1928) The theory of crystal growth. Zeitschrift für physikalische Chemie, 136, 259–278.

Sunagawa, I. (1957) Variation in the crystal habit of pyrite. Geological Survey of Japan Report 175, 1–47.

——— (1981) Characteristics of crystal growth in nature as seen from the morphology of mineral crystals. Bulletin de Minéralogie, 104, 81–87.

Sunagawa, I., and Takahashi, K. (1955) Preliminary report on the relation between the $o(111)$ face of pyrite crystals and its minor contents of arsenic. Geological Society of Japan Bulletin, 6, 1–10.

White, J.S., Jr. (1973) Extreme symmetrical distortion of pyrite from Naica, Mexico. Mineralogical Record, 4, 267–270.

Yamada, S., Nanjo, J., Nomura, S., and Hara, S. (1979) Morphology of iron pyrite crystals. Journal of Crystal Growth, 46, 10–14.

Manuscript received March 9, 1987
Manuscript accepted July 20, 1987